PCCP

PAPER

View Article Online
View Journal | View Issue

Cite this: *Phys. Chem. Chem. Phys.*, 2025, **27**, 18179

Single atom catalysts on the Cr_2NO_2 MXene for CO oxidation

María Guadalupe Moreno-Armenta, *[a] Rodrigo Ponce-Perez, [a] Francesc Viñes *[b] and Lourdes Mestres [c]

Received 20th May 2025,
Accepted 1st August 2025

DOI: 10.1039/d5cp01903f

rsc.li/pccp

Using density functional theory, this work investigates the adsorption of carbon monoxide (CO) molecules and their subsequent oxidation to carbon dioxide (CO_2) on the MXene Cr_2NO_2 decorated with a single atom of transition metal (Sc, V, and Ti) *via* the Eley–Rideal mechanism. The dynamic stability of the MXene is evaluated through phonon calculations, and the thermal stability of the structure is determined by *ab initio* molecular dynamics simulations. First, an oxygen (O_2) molecule is adsorbed onto the metal atom. Sc and Ti induce a partial dissociation, while V causes a full decomposition into atomic O. For the first CO oxidation, all transition metals favor CO oxidation, with Ti and V providing higher and lower activation energies, respectively. However, in the second CO oxidation, the V site is poisoned since the CO_2 molecule is unstable compared to the adsorbed CO. In the case of Ti and Sc, CO_2 formation is feasible, with Sc providing the lowest activation energies. Thus, the present study demonstrates Sc SACs on Cr_2NO_2 as improved catalysts for CO oxidation reactions.

1. Introduction

During the 1960s, new ternary carbides and nitrides were discovered,[1–3] with the general formula: $M_{n+1}AX_n$ (MAX), with n = 1 to 3, M being an early transition metal; A is a p-group element, mainly from groups 13 and 14, while X = C or N. From these MAX compound precursors, a new family of two-dimensional (2D) compounds was discovered in 2011, MXenes, so named for their similarity to graphene.[4] The most common MXene synthesis relies on stripping or selective exfoliation of the A element, *e.g.*, using hydrofluoric acid (HF), although novel F-free synthetic routes have been proposed.[5] Thus, MXenes have a general formula of $M_{n+1}X_nT_x$, where T_x represents the MXene surface terminations resulting from the synthesis. Indeed, the different synthetic methods may influence the MXene morphology and the concomitant physicochemical properties, making them easily tunable compounds useful in multiple applications.[6] Such MXenes exhibit large surface areas, adjustable properties, biocompatibility, and hydrophilicity.[7] They also have excellent electrical, electrochemical, catalytic, and mechanical properties.[8–10] Their layered structure, surface terminations, and selective generation of vacancies make them outstanding materials for many applications, ranging from Li-based batteries,[11] electromagnetic interference (EMI) shielding materials,[12] and carbon dioxide (CO_2) scrubber materials,[13] among many others.

One of the novel applications of MXenes is to use them as a support to single-atom catalysts (SACs),[14] especially when deposited on O-terminated MXenes.[15] SACs, having isolated individual atoms dispersed on a support material, maximize the catalyst exposure while allowing for precise control over the catalyzed reaction, *i.e.*, in principle, all catalytic active sites are well-defined and equivalent, although one should regard that the SAC is biased by its surrounding.[16] Over the last decade, researchers have explored different support materials and coordination environments to enhance the performance and durability of SACs. Recent investigation focused on controlling the hybridization of single atoms in their host materials,[17–19] attracting extensive attention in heterogeneous catalysis given their high catalytic activity, used, for example, in the removal of atmospheric pollutants such as carbon monoxide (CO).[20]

CO is indeed a molecule often produced by the poor combustion of some fuels or compounds, such as gasoline, coal, oil, tobacco, wood, *etc.*, and is also quite toxic for all living beings that breathe oxygen (O_2). Because of this, materials for CO capture, and even better, its catalytic conversion are sought, involving typically transition metal oxides or transition metals (TMs).[21,22] Indeed, the CO oxidation to CO_2 is a classic reaction in heterogeneous catalysis, where traditional catalysts are often late TMs like platinum (Pt), palladium (Pd), gold (Au), rhodium (Rh), and

[a] *Centro de Nanociencias y Nanotecnología, Universidad Nacional Autónoma de México, AP 14, Ensenada, Baja California 22860, Mexico. E-mail: moreno@ens.cnyn.unam.mx*
[b] *Departament de Ciència de Materials i Química Física & Institut de Química Teòrica i Computacional (IQTCUB), Universitat de Barcelona, c/Martí i Franquès 1, 08028 Barcelona, Spain. E-mail: francesc.vines@ub.edu*
[c] *Departament de Química Inorgànica i Orgànica, Secció de Química Inorgánica e Institut de Nanociència i Nanotecnologia (IN2UB), Universitat de Barcelona, c/Martí i Franquès 1, 08028 Barcelona, Spain*

ruthenium (Ru), which are quite effective yet expensive due to their scarcity, and also they require often high working temperatures, limiting their practical applications. Extensive ongoing research is being conducted to identify inexpensive catalysts that could carry out this CO oxidation in an efficient manner yet under mild reaction conditions. TM-based catalysts and other novel materials, such as few-layered two-dimensional TM carbonitrides (MXenes), are being studied to address the limitations of traditional noble metal catalysts while offering effective, low-cost solutions for CO emission control across a range of applications.[23,24] Cai *et al.*[25] have recently reported the catalytic oxidation of the CO molecule using the Zr_2CO_2 MXene decorated with Sc and Ti TMs, with the best results shown for Ti. On the other hand, Zhu *et al.*[26] reported that Ti_2CO_2 decorated with Fe is an excellent catalyst for CO oxidation. Gouveia *et al.*[27] doped the Mo_2CO_2 MXene with Ti, Fe, and Zn; their findings show that the Fe SAC is the most promising candidate for CO oxidation, followed by the Zn SAC. While C-based MXenes have received significant attention, N-based ones are relatively less studied despite showing great promise due to their stability, unique properties, and possible technological applications.[28–32] In this work, we investigated, by density functional theory (DFT) means, the adsorption of CO and the CO_2 formation on the Cr_2NO_2 MXene decorated with a single atom of transition metal (Sc, V, and Ti). We only focused on those early TMs since they are cheaper in comparison with noble metals, which usually require high working temperatures. Additionally, we avoid magnetic TMs since the effect of spin on CO oxidation is a topic of interest that we must address separately.

2. Computational details

By first-principles total-energy calculations, we investigated the adsorption of CO molecules onto the Cr_2NO_2 MXene basal (0001) surface decorated with Sc, V, and Ti TM atoms. Calculations were performed within the DFT framework as implemented in the Vienna *ab initio* simulation package (VASP) code.[33,34] The exchange–correlation energy is treated according to the generalized gradient approximation (GGA) using the Perdew–Burke–Ernzerhof (PBE) exchange–correlation functional,[35] as extensively used in the past for estimating the energies of MXene-based systems.[28,36] Since Cr has highly localized d electrons, the Hubbard correction (DFT+U)[37] was considered to employ the simplified (rotationally invariant) approach introduced by Dudarev *et al.*[38] with U = 3.0 eV, as in previous reports.[31] The electron–ion interaction is modeled employing the plane augmented wave (PAW) method,[39] with an energy cutoff of 460 eV. The dispersive forces have been considered by using Grimme's D3 correction,[40] especially adequate when estimating the interaction of atoms or molecules on MXene surfaces.[41,42] A $p(3 \times 3)$ supercell has been employed in the calculations with a vacuum space of 15 Å, enough to avoid interactions between periodically repeated slabs. During the geometry optimizations, all force components and energy differences were set to be lower than 0.01 eV Å^{-1} and 1×10^{-4} eV, respectively, when reaching convergence. The Brillouin space was sampled with an optimal Monkhorst–Pack k-point mesh of $3 \times 3 \times 1$ size.[43] To investigate the reaction path for the adsorption of CO and the formation of CO_2, the climbing-image nudged-elastic-band (CI-NEB) was used with five intermediate images.[44] Besides, non-covalent interactions (NCIs) were investigated by employing Critic2 software,[45,46] and *ab initio* molecular dynamics (AIMD) calculations were used to investigate the thermal stability of bare MXenes and MXenes containing SACs. The AIMD simulations were carried out in the NVT ensemble using the Nose–Hover thermostat at 300 K, with a step value of 5 fs for a total AIMD simulation time of 5 ps.

3. Results and discussion

3.1. Cr_2NO_2 MXene

The cell parameter of the Cr_2NO_2 MXene (*cf.* Fig. 1a) has been calculated to be 2.95 Å, in good agreement with previous reports.[29,31] This compound exhibits a ferromagnetic behavior with a Cr magnetic moment of $2.47\mu_B$, with each Cr six-fold coordinated with three O and three N, each acquiring an induced magnetization of $-0.12\mu_B$. Regarding electronic properties, the MXene shows half-metal character with the majority spin (spin-up) working as a metal and the minority spin (spin down) as a semiconductor with an estimated indirect Γ–M band gap of 2.76 eV, a feature also observed in other MXenes.[47] Fig. 1b shows the electronic band structure along the Γ–M–K–Γ path with the Fermi energy level, E_F, as a reference. Notice that the conduction channels for spin-up around E_F are mainly composed of the Cr orbitals. The dynamic stability of the MXene is evaluated through phonon calculations and the results are displayed in Fig. 1c, revealing only positive frequencies, indicating their stability. Additionally, we conducted AIMD calculations at 300 K to evaluate the thermal stability of the structure. The variations of temperature and energy are shown in Fig. 1d. Notice that the structure is preserved after the simulation without broken bonds. Both phonon dispersion calculations and AIMD simulations indicate the dynamic and thermal stability of the Cr_2NO_2 MXene.

3.2. MXene decorated with TM atoms

Different TMs (TM = Sc, Ti, or V) were adsorbed onto the surface of the Cr_2NO_2 MXene, considering three different high-symmetry sites: on top of a surface O, a three-fold hollow site with a N underneath (H3), or with a Cr underneath (T4); see Fig. 1a. Once the structures were fully relaxed, we calculated the adsorption energy, E_{ads}, as follows:

$$E_{ads} = E^{sys} - E^{bare} - E^{TM}_{isolated}, \quad (1)$$

where E^{sys}, E^{bare}, and $E^{TM}_{isolated}$ are the total energies of the system at hand, the bare Cr_2NO_2 MXene, and an isolated TM atom, respectively. Besides, the TM cohesive energy, E_{coh}, is calculated as follows:

$$E_{coh} = E^{TM}_{bulk} - E^{TM}_{isolated}, \quad (2)$$

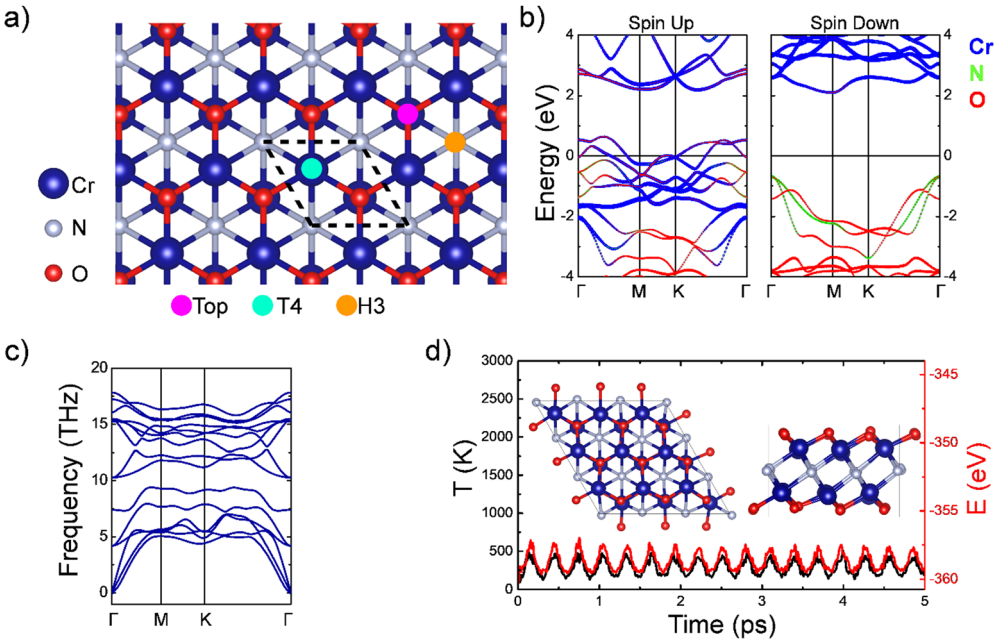

Fig. 1 (a) Top view of the Cr_2NO_2 MXene. The basic unit cell $p(1 \times 1)$ is shown in black, and high-symmetry adsorption sites are also shown. (b) Cr_2NO_2 MXene band structure along the Γ–M–K–Γ path, (c) phonon dispersion and (d) AIMD calculations showing the time evolution of temperature and energy.

where E_{bulk}^{TM} is the total energy of a TM atom in its bulk structure.

These estimated values are summarized in Table 1. In all cases, negative E_{ads} values are obtained, which indicates favorable adsorption. Besides, the H3 site is the most stable site for TM adsorption with binding energies of −9.53, −9.05, and −7.20 eV for Sc, Ti, and V, respectively, given the lower coulombic repulsion with the underlying N layer, located farther away. The comparison of E_{ads} with E_{coh} determines whether the adsorbed atoms would be energetically driven to form clusters on the surface or rather prefer to be well dispersed on the MXene. In all cases, E_{ads} values are lower than E_{coh} values by 2–4 eV, underscoring Cr_2NO_2 as an excellent support for such SACs. Also, the Bader charge was calculated, revealing that, as the number of valence electrons increases, the SAC atom tends to share fewer electrons with the substrate. All this behavior is consistent with a similar trend observed for C-based, O-terminated MXenes.[15]

The electronic properties of these doped systems were also investigated using the projected density of states (PDOS; see Fig. 2), with distinction for the two spin channels. In all cases, the ferromagnetic (FM) character of Cr_2NO_2 is preserved. In the Sc-doped system, the Sc 3d orbital contribution is observed at ∼1.3 eV, with the half-metal property preserved, as in the Ti-doped system, yet the Ti 3d orbitals at ∼1 eV. Finally, for V electronic states at the Fermi level for the minority spin appear, inducing metallic character, with V 3d orbitals at −0.90 and ∼1 eV. Notice also that as the number of valence electrons increases, the contribution to the PDOS of the TM atoms increases. AIMD simulations (*cf.* Fig. 2) on the doped systems reveal non-broken bonds, a preserved structure geometry, and thermal stability.

Table 1 Adsorption energies (E_{ads}, in eV) for Sc, Ti, and V at different high-symmetry sites of Cr_2NO_2, as well as cohesive energies (E_{coh}, in eV), and SAC Bader charges (Q, in e)

	E_{ads}/eV				
TM	Top	T4	H3	E_{coh}/eV	Q/e
Sc	−5.58	−9.24	−9.53	−4.49	1.89
Ti	−4.94	−8.85	−9.05	−5.79	1.85
V	−4.03	−6.89	−7.20	−5.91	1.70

3.3. Oxygen adsorption

CO oxidation is investigated *via* the Eley–Rideal (ER) mechanism. An O_2 molecule is first adsorbed on the TM-anchored MXene in this mechanism. After that, the CO molecules interact with the adsorbed O atoms to desorb two CO_2 molecules. Fig. 3 presents the minimum energy pathway (MEP) for the adsorption and activation of the O_2 on Sc, Ti, or V SACs. The zero energy (ZS) reference is set when the molecule and substrate are far enough to not interact. In all cases, O_2 is found to absorb barrierless. Once the O_2 molecule is adsorbed onto the metal atom (O_2* stage), the adsorption energy, E_{ads}, is defined as follows:

$$E_{ads} = E_{sys} - E_{subs} - E_{mol}. \quad (3)$$

The first, second, and third terms on the right-hand side of the equation refer to the total energy of the O_2* system, the TM@Cr_2NO_2 substrate, and the isolated molecule, respectively. The E_{ads} values are −1.70, −3.23, and −3.45 eV for Sc, Ti, and V SACs, respectively. On the other hand, the E_{ads} values for the CO molecules are −0.40, −1.08, and −1.47 eV for Sc, Ti, and V SACs, respectively. These energies are lower compared to O_2; therefore, the ER mechanism is feasible. The activation energy to dissociate the O_2* into 2O* (E_{act1}) is found to be 2.89, 1.03,

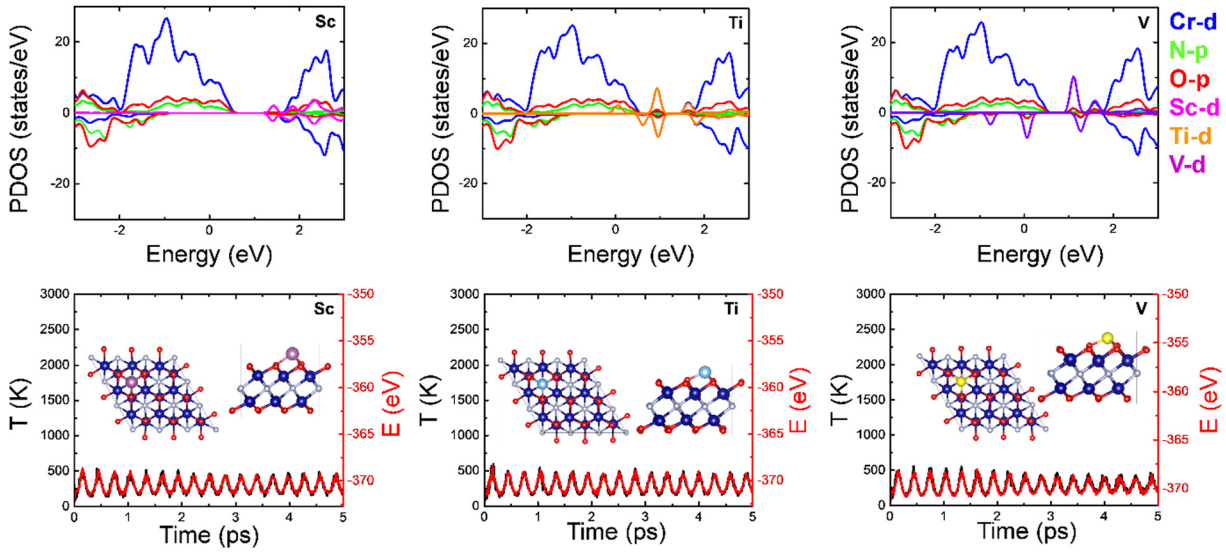

Fig. 2 PDOS and AIMD simulations at 300 K for the Sc-, Ti-, and V-doped Cr_2NO_2 MXenes. In the latter case, insets show the top and side views of the doping atoms on Cr_2NO_2, with Sc, Ti, and V atoms shown as purple, cyan, and yellow spheres, respectively.

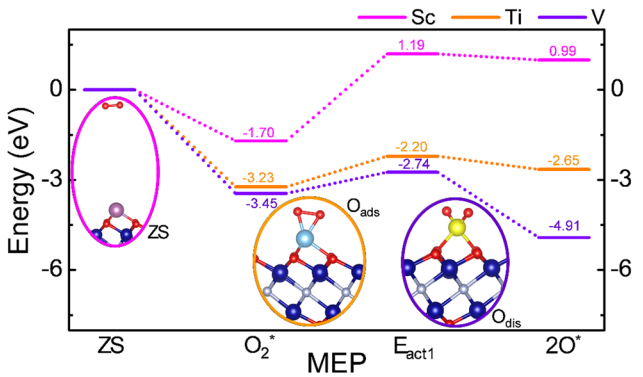

Fig. 3 MEP of O_2 adsorption and dissociation on the SAC@Cr_2NO_2 MXene models, with side views of the different reaction stages, including ZS, O_2*, E_{act1}, and 2O*.

and 0.69 eV for Sc, Ti, and V, respectively, implying that it is more difficult for the earlier TMs. Additionally, the reaction step is endothermic by 2.69, 0.58, and −1.46 eV for Sc, Ti, and V, revealing that the difficulty in breaking O_2 on the Sc SAC is mostly thermodynamic, while this step is more affordable for Ti and V, since the final state is below the energy reference, and also the reaction step is exothermic on the V SAC.

Note that once O_2 is adsorbed, the interaction with the SAC is so strong that it weakens the molecular bond, as evidenced by the interatomic distance d(OO) of 1.38, 1.48, and 1.44 Å for Sc, Ti, and V SACs, elongated by at least 0.15 Å from the gas phase value of 1.23 Å. The electron localization function (ELF) line along the O–O bond shows a decrease in the electron population (*cf.* Fig. S1 of the SI). Thus, even if O_2 dissociation would be costly on Sc and Ti, the bond weakening implies O_2* activation, and so the CO oxidation on them could be envisioned.

3.4. First CO oxidation

Once O_2 is adsorbed, activated, or broken on the metal atom, the second step is the oxidation of a CO molecule to form CO_2. Fig. 4 depicts this minimum energy path (MEP), where the initial stage (IS) is when the CO molecule is far away from the O_2* system. First, the CO molecule adsorbs onto the SAC/MXene with the O_2* or 2O*, *i.e.* the CO* stage, with E_{ads} of −0.73, −0.54, and −0.18 eV for Sc, Ti, and V SACs, respectively. From this, CO_2 can be formed surpassing energy barriers of 0.96, 1.45, and 0.66 eV for Sc, Ti, and V, respectively, *i.e.* the E_{act2} stage. Note that the V SAC provides a lower activation energy, which goes along with the lower full dissociation O_2 molecule, while the Ti SAC has a higher activation energy, which could be associated with the large O_2 E_{ads} of −3.23 eV. In all cases, CO oxidation is favorable with a gain of energy larger than ∼2.5 eV when forming CO_2, *i.e.* the CO_2* stage. However, at this point, the CO_2 molecule remains adsorbed onto the MXene SAC. Therefore, as a final step, *i.e.* the CO_2(g)

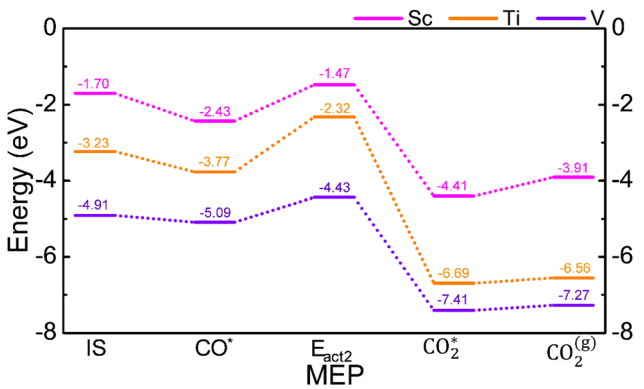

Fig. 4 MEP of CO oxidation on O_2* or 2O* on SAC/Cr_2NO_2, including CO*, CO_2*, and CO_2*(g) stages.

stage, the CO_2 desorption is calculated as the inverse of the adsorption energy, with small values of −0.50, −0.13, and −0.13 eV for Sc, Ti, and V, implying that it would be easy to desorb CO_2.

The atomic representation of the different steps for the first CO oxidation is displayed in Fig. 5. Also, the non-covalent interactions[48] between molecules and substrates are investigated. The figure shows the reduced gradient, s, isosurface with an isovalue of s = 0.5 a.u. (color coding: red and blue indicate repulsive and attractive interactions, respectively, while green regions denote van der Waals (vdW) interactions). The far CO or CO_2 situations are not shown, since there is no interaction with the catalyst.

In the CO* stage, the NCI shows that the CO molecule is interacting with the surface MXene mainly through vdW-type interactions; besides, in the Ti SAC, a large isosurface is observed, which indicates a strong molecule/substrate interaction, followed by the Sc and V cases. The graphs of s *vs.* sign(λ_2)ρ shown in Fig. S2 of the SI show that, in the Ti SAC, a repulsive interaction between Ti and CO is characterized by the peak at 0.05 a.u. at low s. This repulsive interaction seems to be the origin of the high activation energy, since such an interaction does not appear in the Sc and V cases.

Notice that, in the E_{act2} state, the vdW interactions between molecules and the substrate are reduced compared to CO*. However, the interaction is centered between the transition metal and molecule, as evidenced in Fig. 5. In the Sc SAC, the CO molecule is interacting with the O adsorbed onto the Sc with a C–O distance of 1.62 Å, and the s *vs.* sign(λ_2)ρ graph shows peaks at ±0.17 a.u. at low s, evidencing the charge transference between atoms and forming the C–O bond; see Fig. S2 of the SI. In a similar way, the V SAC shows a peak at ±0.1 a.u. (*cf.* Fig. S2 of the SI), which corresponds with a bond formation between C and O with a d(CO) of 1.77 Å. In the case of the Ti SAC, it is noticed that, at the transition state, a pseudo-CO_2 molecule is formed with a d(CO) of 1.18 Å; Fig. S2 of the SI corroborates the bond formation because a peak is located at ±0.2 a.u. at a reduced gradient. However, the molecule remains anchored with the TM. To corroborate the CO_2 formation, Fig. S3 of the SI shows 2D charge density plots at the transition state. Finally, in the CO_2* state, regardless of the case, the CO_2 molecule interacts with the TM through vdW forces, as corroborated in Fig. S2 of the SI.

3.5. Second CO oxidation

Once the first CO_2 molecule is desorbed, the next step is the adsorption and subsequent oxidation of a second CO molecule. Fig. 6 shows the reaction mechanism, where the middle stage (MS) is when the second CO molecule is far away from the MXene. The CO E_{ads} is favorable by −0.61, −0.50, and −0.25 eV for Sc, Ti, and V SACs, *i.e.* the $CO_{(II)}$* stage. Once CO* is formed, it reacts with the O* on the SAC, with energy barriers of 0.72 and 0.80 eV for Ti and V SACs, respectively, *i.e.* the E_{act3} stage. Notice that the formation of the second CO_2, *i.e.* the $CO_{(2II)}$* stage, is 0.51 eV less stable than adsorbed CO in the V-based SAC, which suggests that the V site is poisoned for the second CO oxidation step. In the case of the Ti SAC, the CO_2* is 0.24 eV more stable than CO*, evidencing the feasibility to form CO_2. Regarding the Sc SAC, the activation energy to form CO_2 is 0.02 with a gain of energy of 2.72 eV. The desorption energies for CO_2*, *i.e.* the $CO_{2(II)}$ stage, are 0.69, 0.75, and 0.47 eV for Sc, Ti, and V SACs, respectively.

Fig. 7 shows the atomic representation of the different stages of the second CO oxidation, including the reduced gradient isosurfaces with s = 0.5 a.u. similar to the previous case, except for the non-interacting MS and $CO_{2(II)}$. In all cases for $CO_{(II)}$*, the CO molecule mainly interacts through vdW interactions, in line with E_{ads} values. Besides the observed attractive interactions between the TM and molecule, the s *vs.* sign(λ_2)ρ graph (*cf.* Fig. S4 of the SI) demonstrates that Ti

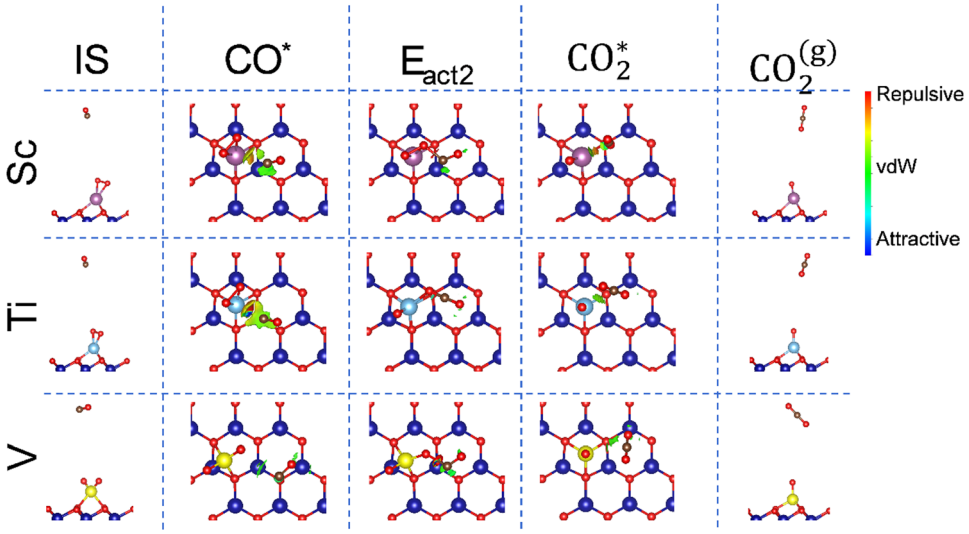

Fig. 5 Side views of IS and CO2(g) states, and top views of CO*, E_{act2}, and CO_2* states, for the first CO oxidation step, with NCI isosurfaces at s = 0.5 a.u., with the color legend shown on the side, for different SAC/Cr_2NO_2.

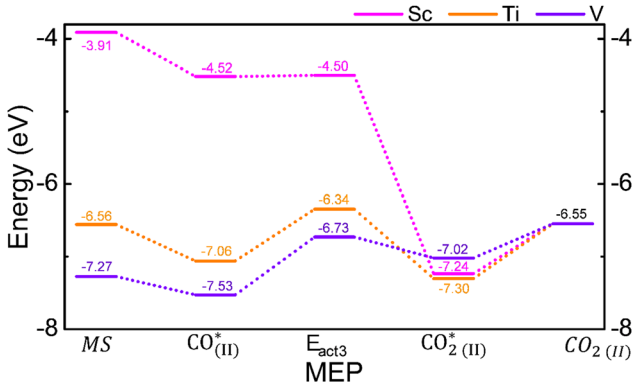

Fig. 6 MEP of CO oxidation on O* on SAC/Cr_2NO_2, including CO*, CO_2*, and CO_2*(g) stages.

experiences a larger attractive interaction towards CO, followed by V and Sc SACs. Also, a more pronounced region of repulsive interaction is observed in the V case, followed by Ti and Sc SACs, which demonstrates why Sc provides the largest E_{ads}. In E_{act3}, the d(CO) bond between the CO molecule and the O* is 1.62 Å for the Ti SAC, with a separation of 1.77 Å between Ti and O atoms. Fig. S4 of the SI shows a peak at −0.18, demonstrating bond formation. In the V SAC case, a d(VO) of 1.22 Å suggests the formation of the CO_2 molecule. Besides, the CO_2 continues to interact with the V atoms due to a distance of 2.08 Å. Also, their corresponding s *vs.* sign(λ_2)ρ graph (*cf.* Fig. S4) demonstrates an attractive interaction between the molecule and V. As far as the Sc SAC is concerned, in the transition state there is an increase in the attractive interaction between the TM and the molecule in comparison with the previous CO oxidation, which is a consequence of a smaller distance between Sc and CO of 2.36 Å. Therefore, one can conclude that once the molecule diffuses across the substrate to be closer enough to Sc, the formation of CO_2 becomes spontaneous. Fig. S5 of the SI shows the charge distribution maps for the transition state. In the Ti and V SACs, the CO_2 formation is clearly observed. However, the oxygen atom remains attached to Ti, while in the V case only the interaction weakens. Finally, in $CO_{2(II)}$* the three different systems exhibit similar behavior since the CO_2 molecule continues to attractively interact with the TM, corroborated by the peak observed at −0.05 in their corresponding s *vs.* sign(λ_2)ρ graphs.

Cai *et al.*[25] reported CO oxidation through the ER mechanism on Sc@Zr_2CO_2 and Ti@Zr_2CO_2 SACs. In both cases, the first CO_2 formation was feasible with activation energies of 1.06 and 0.65 eV, respectively. However, the second CO_2 formation was unstable in Ti@Zr_2CO_2, while it was viable in Sc@Zr_2CO_2 with activation energies of 0.17 eV. Zhang and coworkers[49] reported the Ti@Ti_2CO_2 catalyst for CO oxidation; the results showed the feasibility of forming the first CO_2 molecule with an activation energy of 0.25 eV. However, in the second CO_2 formation, the SAC was poisoned, as CO_2 formation was less stable than CO adsorbed on the MXene. On the other hand, Talib *et al.*[50] employed the Ru@Mo_2CS_2 and Ir@Mo_2CS_2 MXenes for CO oxidation; their findings showed that in the ER mechanism, the first activation energy was 0.52 eV (51 eV) for the Ru (Ir) SAC, while for the 2nd CO_2 formation, the activation energies were 0.80 and 0.61 eV, respectively. Similarly, Fe@Ti_2CO_2 provided activation energies of 0.77 eV and 0.13 eV for the first and second CO_2 oxidations in the ER mechanism, respectively.[26] Our findings show that Ti and Sc SACs facilitate the complete oxidation of CO, thereby enhancing the use of Cr_2NO_2 as a substrate for SACs.

4. Conclusions

Our results show that the Cr_2NO_2 MXene has half-metal character and exhibits dynamic and thermal stability. The most

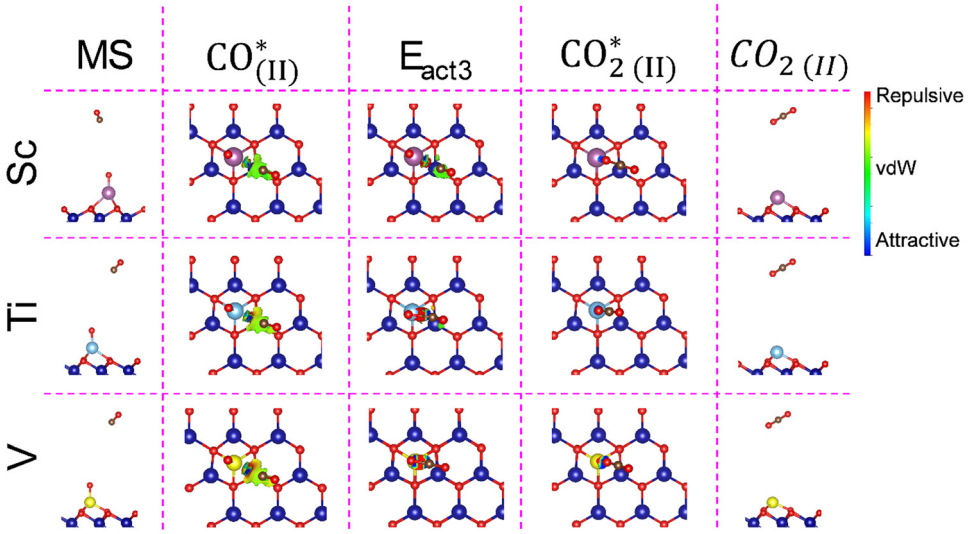

Fig. 7 Side views of CO(g) and CO_2(g), and top views of CO*, the transition state, and CO_2*, for the second CO oxidation step, with NCI isosurfaces at s = 0.5 a.u., with the color legend shown on the side, for the different SAC/Cr_2NO_2.

favorable site for the adsorption of Sc, Ti, and V is in the H3 site. In all cases, the adsorption energy values are lower than the SAC bulk metal cohesive energy values, which indicates that the transition metal atoms would be thermodynamically driven to remain as isolated atoms, and so to behave as single-atom catalysts. In all the doped cases, the ferromagnetic behavior of the substrate and its thermal stability are preserved. The validity of the Eley–Rideal mechanism used to investigate the oxidation of CO is confirmed by the present DFT results. The O_2 molecule is adsorbed on the MXene-anchored SAC, and the O_2 activation occurs with a molecular bond either weakened or completely dissociated, which promotes CO oxidation. For the first CO adsorption, the NCI shows that the molecule is interacting with the MXene surface mainly through vdW interactions; besides, in the Ti SAC, a large isosurface is observed, which indicates a strong molecule/substrate interaction, followed by the Sc and V cases. In the Ti SAC, a repulsive interaction between Ti and the CO occurs. This repulsive interaction causes the largest activation energy of 1.75 eV in the Ti case, since such an interaction does not occur in the Sc and V cases. For this reason, the d(CO) in Ti is significantly shorter. For the second CO oxidation, the molecule is adsorbed *via* vdW forces, then it interacts with the oxygen in the TM atom to form CO_2. In the V case, the formation of the second CO_2 is less stable than the adsorbed CO, which points to a poisoned V site; thus, the second CO oxidation is unfavorable. In the case of Sc, once the molecule is adsorbed, an attractive interaction between the Sc and CO forces the CO to diffuse toward Sc and the formation of CO_2 is spontaneous. In the Ti and V SACs, the CO_2 is formed. However, the oxygen atom remains attached to Ti, while in the V case, it interacts only weakly. Our calculations demonstrate that the Sc SAC provides better results for the CO oxidation with a first activation energy of 0.96 eV and the second CO_2 formation being essentially barrierless. This could be attributed to the low population of valence electrons and substantial large electron transfer between the TM and the substrate.

Conflicts of interest

There are no conflicts to declare.

Data availability

The data supporting this article have been included as part of the SI. Supplementary information available: ELF line profiles along O–O bond; the *s vs.* sig(λ_2)ρ plots for the first CO oxidation; charge density differences along the C–O bond; the *s vs.* sig(λ_2)ρ plots for the second CO oxidation; charge distribution along the TM–O–C–O bonds. See DOI: **https://doi.org/10.1039/d5cp01903f**

Acknowledgements

M. G. Moreno thanks PASPA DGAPA UNAM for her sabbatical funding support. Calculations were performed in the DGCTIC-UNAM Supercomputing Center (projects LANCAD-UNAM-DGTIC-150 and LANCAD-UNAM-DGTIC-422). We thank DGAPA-UNAM for partial financial support (IN101523, IA100226 and IA100624). This study has been supported by the Spanish Ministerio de Ciencia e Innovación and Agencia Estatal de Investigación (AEI) MCIN/AEI/10.13039/501100011033 through projects PID2021-126076NB-I00, TED2021-129506B-C22, la Unidad de Excelencia María de Maeztu CEX2021-001202-M granted to the IQTCUB and, in part, from COST Action CA18234, and Generalitat de Catalunya 2021SGR00079. F. V. is thankful for the ICREA Academia Award 2023 Ref. Ac2216561. L. M. thanks projecte 2023 CLIMA 00009 amb el suport del Departament de Recerca i Universitats: del Departament d'Acció Climàtica, Alimentació i Agenda Rural; i del Fons Climàtic de la Generalitat de Catalunya.

References

1 W. Jeitschko, H. Nowotny and F. Benesovsky, Carbides of Formula T_2MC, *J. Less-Common Met.*, 1964, **7**, 133–138.
2 M. W. Barsoum, The $M_{N+1}AX_N$ Phases: A New Class of Solids; Thermodynamically Stable Nanolaminates, *Prog. Solid State Chem.*, 2000, **28**, 201–281.
3 M. W. Barsoum and T. El-Raghy, Synthesis and Characterization of a Remarkable Ceramic: Ti_3SiC_2, *J. Am. Ceram. Soc.*, 1996, **79**, 1953–1956.
4 M. Naguib, M. Kurtoglu, V. Presser, J. Lu, J. Niu, M. Heon, L. Hultman, Y. Gogotsi and M. W. Barsoum, Two-Dimensional Nanocrystals Produced by Exfoliation of Ti_3AlC_2, *Adv. Mater.*, 2011, **23**, 4248–4253.
5 S. Y. Pang, Y. T. Wong, S. Yuan, Y. Liu, M. K. Tsang, Z. Yang, H. Huang, W. T. Wong and J. Hao, Universal Strategy for HF-Free Facile and Rapid Synthesis of Two-Dimensional MXenes as Multifunctional Energy Materials, *J. Am. Chem. Soc.*, 2019, **141**, 9610–9616.
6 B. Anasori and M. Naguib, Two-Dimensional MXenes, *MRS Bull.*, 2023, **48**, 238–244.
7 Y. Gogotsi and B. Anasori, The Rise of MXenes, *ACS Nano*, 2019, **13**, 8491–8494.
8 A. Zhou, Y. Liu, S. Li, X. Wang, G. Ying, Q. Xia and P. Zhang, From Structural Ceramics to 2D Materials with Multi-Applications: A Review on the Development from MAX Phases to MXenes, *J. Adv. Ceram.*, 2021, **10**, 1194–1242.
9 J. Zhu, E. Ha, G. Zhao, Y. Zhou, D. Huang, G. Yue, L. Hu, N. Sun, Y. Wang, L. Y. S. Lee, C. Xu, K.-Y. Wong, D. Astruc and P. Zhao, Recent Advance in MXenes: A Promising 2D Material for Catalysis, Sensor and Chemical Adsorption, *Coord. Chem. Rev.*, 2017, **352**, 306–327.
10 A. Lakmal, P. B. Thombre and C. E. Shuck, Solid-Solution MXenes: Synthesis, Properties, and Applications, *Acc. Chem. Res.*, 2024, **57**, 3007.
11 X. Tang, X. Guo, W. Wu and G. Wang, 2D Metal Carbides and Nitrides (MXenes) As High-Performance Electrode Materials for Lithium-Based Batteries, *Adv. Energy Mater.*, 2018, **8**, 1801897.
12 M. Han, C. E. Shuck, R. Rakhmanov, D. Parchment, B. Anasori, C. M. Koo, G. Friedman and Y. Gogotsi, Beyond

$Ti_3C_2T_x$: MXenes for Electromagnetic Interference Shielding, *ACS Nano*, 2020, **14**, 5008–5016.
13 R. Morales-Salvador, Á. Morales-García, F. Viñes and F. Illas, Two-Dimensional Nitrides as Highly Potential Candidates for CO_2 Capture and Activation, *Phys. Chem. Chem. Phys.*, 2018, **20**, 17117–17124.
14 B. Qiao, A. Wang, X. Yang, L. F. Allard, Z. Jiang, Y. Cui, J. Liu, J. Li and T. Zhang, Single-Atom Catalysis of CO Oxidation Using Pt_1/FeO_x, *Nat. Chem.*, 2011, **3**, 634–641.
15 M. Keyhanian, D. Farmanzadeh, Á. Morales-García and F. Illas, Effect of Oxygen Termination on the Interaction of First Row Transition Metals with M2C MXenes and the Feasibility of Single-Atom Catalysts, *J. Mater. Chem. A*, 2022, **10**, 8846–8855.
16 G. Di Liberto, L. A. Cipriano and G. Pacchioni, Effect of Oxygen Termination on the Interaction of First Row Transition Metals with M_2C MXenes and the Feasibility of Single-Atom Catalysts, *ChemCatChem*, 2022, **14**, e202200611.
17 T. Wang, Y. Sun, G. Fu, Z. Jiang, X. Zheng, J. Li and Y. Deng, Progress of Main-Group Metal-Based Single-Atom Catalysts, *Electrochem. Energy Rev.*, 2024, **7**, 1–34.
18 N. Cheng, L. Zhang, K. Doyle-Davis and X. Sun, Single-Atom Catalysts: From Design to Application, *Electrochem. Energy Rev.*, 2019, **2**, 539–573.
19 J. D. Gouveia, H. Rocha and J. R. B. Gomes, MXene-Supported Transition Metal Single-Atom Catalysts for Nitrogen Dissociation, *Mol. Catal.*, 2023, **547**, 113373.
20 D. D. Singh, A. Mohan, A. Walia, D. Choudhary and K. L. A. Khan, A Concept for Removing the Pollutants from Air, *Mater. Today: Proc.*, 2022, **64**, 1539–1542.
21 K. Wang, Y. Shen, L. Lv, X. Meng, X. Jiang, L. Pang, P. E and Z. Zhou, First Principles Study of Transition Metal (TM = Sc, Ti, V, Cr, Mn) Doped Penta-BAs_5 Monolayer for Adsorption of CO, NH_3, NO, SO_2, *FlatChem*, 2024, **46**, 100668.
22 H. A. Tahini, X. Tan and S. C. Smith, Facile CO Oxidation on Oxygen-Functionalized MXenes *via* the Mars-van Krevelen Mechanism, *ChemCatChem*, 2020, **12**, 1007–1012.
23 Q. Peng, X. Zhang, Z. Geng, Z. Yang and J. Yang, Single Zn Atom Catalyst on Ti_2CN_2 MXenes for Efficient CO Oxidation, *Phys. E*, 2023, **147**, 115595.
24 B. Cai, J. Zhou, D. Li and Z. Ao, Humidity Tuning CO Oxidation on Ti decorated V_2CO_2 Monolayer (MXene) Catalyst: A Density Functional Calculation Study, *Appl. Surf. Sci.*, 2023, **616**, 156497.
25 B. Cai, J. Zhou, D. Li and Z. Ao, New Insights into the Single-Atom-Decorated Zr_2CO_2 (MXene) as an Efficient Catalyst for CO Oxidation in Incomplete Combustion Gas, *Appl. Surf. Sci.*, 2022, **575**, 151777.
26 C. Zhu, J. X. Liang, Y. G. Wang and J. Li, Non-noble metal single-atom catalyst with MXene support: Fe1/Ti2CO2 for CO oxidation, *Chin. J. Catal.*, 2022, **43**, 1830.
27 J. D. Gouveia and J. R. B. Gomes, Single-Atom Catalysts Based on the Mo2CO2 MXene for CO Oxidation, *Adv. Theory Simul.*, 2024, **7**, 2400342.
28 R. Morales-Salvador, Á. Morales-García, F. Viñes and F. Illas, Two-Dimensional Nitrides as Highly Efficient Potential Candidates for CO_2 Capture and Activation, *Phys. Chem. Chem. Phys.*, 2018, **20**, 17117.
29 R. Ponce-Pérez, J. Guerrero-Sánchez, S. J. Gutiérrez-Ojeda and M. G. Moreno-Armenta, Oxygen Coverage Effect on the Magnetic Properties of the Cr_2NO_x ($0 \leq x \leq 2$) MXene, *ACS Appl. Electron. Mater.*, 2021, **3**, 4967–4976.
30 S. J. Gutiérrez-Ojeda, R. Ponce-Pérez, D. Maldonado-López, D. M. Hoat, J. Guerrero-Sánchez and M. G. Moreno-Armenta, Strain Effects on the Two-Dimensional Cr_2N MXene: An *Ab Initio* Study, *ACS Omega*, 2022, **7**, 33884–33894.
31 R. Ponce-Pérez, J. Guerrero-Sánchez, S. J. Gutiérrez-Ojeda, H. N. Fernández Escamilla, D. M. Hoat and M. G. Moreno-Armenta, A Candidate Exchange-Biased vdW Heterostructure Based on Cr_2NO_2 and Cr_2CF_2 MXenes, *Mater. Today Electron.*, 2023, **6**, 100059.
32 S. J. Gutiérrez-Ojeda, R. Ponce-Pérez, J. Guerrero-Sánchez and M. G. Moreno-Armenta, MXene Heterostructures Based on Cr_2C and Cr_2N: Evidence of Strong Interfacial Interactions that Induce an Antiferromagnetic Alignment, *Graphene 2D Mater.*, 2024, **9**, 47–57.
33 G. Kresse and J. Furthmüller, Efficient Iterative Schemes for *Ab Initio* Total-Energy Calculations Using a Plane-Wave Basis Set, *Phys. Rev. B:Condens. Matter Mater. Phys.*, 1996, **54**, 11169–11186.
34 G. Kresse and J. Furthmüller, Efficiency of *Ab-Initio* Total Energy Calculations for Metals and Semiconductors Using a Plane-Wave Basis Set, *Comput. Mater. Sci.*, 1996, **6**, 15–50.
35 J. P. Perdew, K. Burke and M. Ernzerhof, Generalized Gradient Approximation Made Simple, *Phys. Rev. Lett.*, 1996, **77**, 3865–3868.
36 D. Ontiveros, F. Viñes and C. Sousa, Tuning MXenes Towards Their Use in Photocatalytic Water Splitting, *Energy Environ. Mater.*, 2024, **7**, e12774.
37 V. I. Anisimov, F. Aryasetiawan and I. Lichtenstein, First-Principles Calculations of the Electronic Structure and Spectra of Strongly Correlated Systems: The LDA + U Method, *J. Phys.: Condens. Matter*, 1997, **9**, 767–808.
38 S. Dudarev, G. Botton, S. Y. Savrasov, C. J. Humphreys and A. P. Sutton, Electron-Energy-Loss Spectra and the Structural Stability of Nickel Oxide: An LSDA + U study, *Phys. Rev. B: Condens. Matter Mater. Phys.*, 1998, **57**, 1505–1509.
39 P. E. Blöchl, Projector Augmented-Wave Method, *Phys. Rev. B:Condens. Matter Mater. Phys.*, 1994, **50**, 17953.
40 S. Grimme, J. Antony, S. Ehrlich and H. Krieg, A Consistent and Accurate *Ab Initio* Parametrization of Density Functional Dispersion Correction (DFT-D) for the 94 Elements H-Pu, *J. Chem. Phys.*, 2010, **132**, 154104.
41 J. D. Gouveia, G. Novell-Leruth, P. M. L. S. Reis, F. Viñes, F. Illas and J. R. B. Gomes, First-Principles Calculations on the Adsorption Behavior of Amino Acids on a Titanium Carbide MXene, *ACS Appl. Bio Mater.*, 2020, **3**, 5913–5921.
42 J. D. Gouveia, G. Novell-Leruth, F. Viñes, F. Illas and J. R. B. Gomes, The Ti_2CO_2 MXene as a Nucleobase 2D Sensor: A First-Principles Study, *ACS Appl. Surf. Sci.*, 2021, **544**, 148946.
43 H. J. Monkhorst and J. D. Pack, Special Points for Brillouin-Zone Integrations, *Phys. Rev. B*, 1976, **13**, 5188–5192.
44 G. Henkelman and H. Jónsson, A Climbing Image Nudged Elastic Band Method for Finding Saddle Points and Minimum Energy Paths, *J. Chem. Phys.*, 2000, **113**, 9901–9904.

45 A. Otero-de-la-Roza, E. R. Johnson and V. Luaña, Critic2: A Program for Real-Space Analysis of Quantum Chemical Interactions in Solids, *Comput. Phys. Commun.*, 2014, **185**, 1007.
46 A. Otero-de-la-Roza, M. A. Blanco, Á. Martín Pendás and V. Luaña, Critic: A New Program for the Topological Analysis of Solid-State Electron Densities, *Comput. Phys. Commun.*, 2009, **180**, 157.
47 D. Ontiveros, F. Viñes and C. Sousa, Exploring the Photoactive Properties of Promising MXenes for Water Splitting, *J. Mater. Chem. A*, 2025, **13**, 3302–3316.
48 E. R. Johnson, S. Keinan, P. Mori-Sánchez, J. Contreras-García, A. J. Cohen and W. Yang, Revealing Noncovalent Interactions, *J. Am. Chem. Soc.*, 2010, **132**, 6498–6506.
49 X. Zhang, J. Lei, D. Wu, X. Zhao, Y. Jinga and Z. Zhou, A Ti-anchored Ti2CO2 monolayer (MXene) as a single-atom catalyst for CO oxidation, *J. Mater. Chem. A*, 2016, **4**, 4871.
50 S. H. Talib, Z. Lu, B. Bashir, S. Hussain, K. Ahmad, S. Khan, S. Haider, Z. Yang, K. Hermansson and J. Li, CO oxidation on MXene (Mo2CS2) supported single-atom catalyst: A termolecular Eley-Rideal mechanism, *Chin. Chem. Lett.*, 2023, **34**, 107412.